Selective glucose oxidation to organic acids over synthesized bimetallic oxides at low temperatures

**Hülya A. Kılıç**[1] ⬦ **· Yaşar Gök**[1] ⬦

Abstract

Oxidation of glucose was investigated over bimetallic oxide catalysts with H_2O_2 at 70–90 °C in ethanol and water under atmospheric pressure. Bimetallic oxides, contain Zn, Ce, Al, Mg, Sr and Fe were synthesized with co-precipitation methods. Screening of these oxides were proceeded in ethanol and the most effective one was tested in a more natural solvent water for 6 h. Effects of crystal structure, calcination, metal loading, reaction time and temperature on catalytic activity and product selectivities were investigated. Glucose conversion reactions were also performed with and without O_2 source as comparison. The most active and selective catalyst in ethanol at 70 °C was found as Mg–Al–cal (62% glucose conversion and 10.2% formic acid selectivity). Metal loadings (Cu/V) to Mg–Al–cal lowered the catalytic activity significantly. Mg–Al–cal, tested in water at 90 °C, provided almost 95% of organic acid (formic and acetic acid) selectivity with 38% conversion. Deactivation of Mg–Al–cal by product adsorption was also investigated by the addition of formic acid in ethanol at 70 °C. In the presence of formic acid, the catalyst exhibited 50% of glucose conversion and 78% of total organic acid selectivity (levulinic acid + lactic acid + formic acid) without using O_2 source.

Hülya A. Kılıç and Yaşar Gök have contributed equally to this work.

✉ Yaşar Gök
  yasar.gok@usak.edu.tr

1 Department of Chemical Engineering, Uşak University, 64200 Uşak, Turkey

Graphical abstract
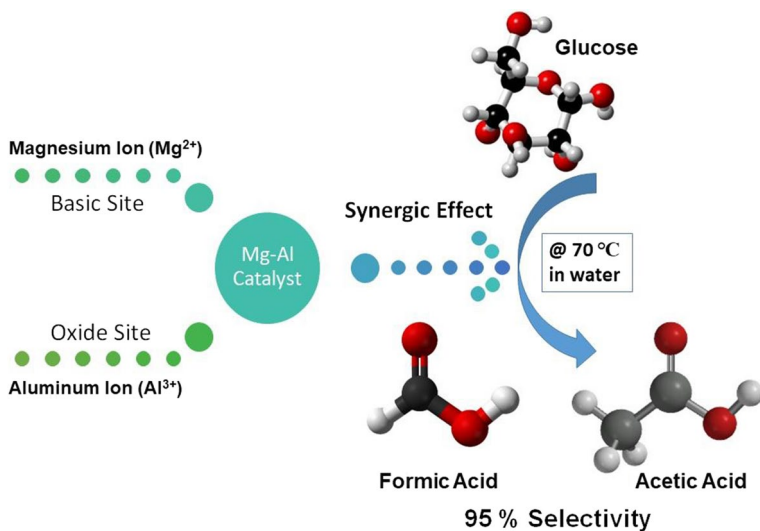
Introduction

Low carbon emission technologies have been attracted much interests at the beginning of the 21th century due to the rising carbon footprint by fossil fuel reserves [1]. That is why production of key chemicals from bio-derived sources is currently challenging [2–7]. Monosaccharides, such as glucose, are promising candidates for the production of many valuable chemicals instead of the fossil resources. Glucose can be evaluated in hydrogenation for sugar alcohols [8–10], in dehydration for furans [11, 12], in retro-aldol condensation for lactic acid and aldehydes [13] and in oxidation for organic acids [14, 15]. Among these processes, oxidation of glucose is of great interest since organic acids are widely used platform chemicals in many industries [16–19].

As an organic acid, formic acid is the main chemical for leather, textile, pharmaceutical and agricultural industries [20]. Formic acid is also a promising hydrogen source since it can be easily decomposed into CO_2 and H_2 [20–22]. The conventional production of formic acid is currently carried out under extreme conditions [20]. In addition, acetic acid is also crucial building-block as a monomer of vinyl acetate with the annual production of 15 million tons [23]. Unfortunately, current production processes for both acids have been emerging high amounts of carbon dioxide emissions [24].

Great efforts have been made in the last decades for the synthesis of acetic and formic acids via oxidation of sugars [25–28]. Few studies provided high selectivities

for the production of these acids [16, 29]. However, they were not achieved via cost effective or environmentally friendly ways. Some functional groups in glucose such as –OH, facilitates its oxidation to these acids. A selective catalyst should possess both base and oxidative sites for oxygen transfer [30, 31]. Many different types of catalysts, including homogeneous bases, were tested in glucose oxidation [26]. Wang and coworkers [29] carried out glucose oxidation with homogeneous bases (LiOH, NaOH, KOH etc.) and H_2O_2 under mild conditions (Room temperature and atmospheric conditions). Almost complete glucose conversion to formic acid was achieved with NaOH. Low temperature and pressure also prevented the decomposition of formic acid. Nevertheless, this method requires significant amounts of homogeneous base. Gromov et al. [6] investigated direct conversion of cellulose to formic acid over Mo and V containing heteropolyacids in a novel study. High yields of formic acid (66%) were achieved at 160 °C and 20 bar. In this study, yield of the formic acid was related to the O_2 pressure. This high pressure was also reported to have positive effects on catalyst activation. On the other hand, economic potential of this method limits its industrial application. Au containing catalysts have been extensively used in oxidation of cellulose derived substrates to gluconic acid [32, 33]. Perfect selectivities (80–100%) were obtained in many detailed studies with molecular O_2 as oxidant regardless of the type of the support. Nevertheless, the future of such catalysts looks doubtful due to the scarcity of gold.

Bimetallic oxides, in spinel and layered double hydroxides (LDH) form, exhibited promising performances on oxidation in earlier researches [16, 34–36]. Choundary et al. [37] synthesized different metal containing LDHs (Co–Al, Co–Cr, Ni–Al, Zn–Al, Mg–Fe, Mn–Fe etc.) to be tested in benzyl alcohol oxidation. Oxidation over Co–Cr–LDH provided ~90% selectivity to target product benzaldehyde at 60% conversion at 70 °C using H_2O_2 as an oxidant. Findings were associated with the bifunctional property of the Co-Cr-LDH: base sites activated the reactant and oxidant where transition sites were responsible for redox/oxidation mechanism. Zou et al. [38] tested Zn–Co LDH catalyst in benzyl alcohol oxidation at 65 °C using TBHP (tert-butyl hydroperoxide) and reported 72% conversion providing 90% of benzaldehyde selectivity. They also achieved the highest catalytic activity value with this catalyst (14.5 mmol/gcat.h) in benzyl alcohol oxidation.

The present research focused on screening of the different synthesized bimetallic catalysts (Sr–Fe, Mg–Al, Zn–Ce etc.) in glucose oxidation to organic acids. It was aimed to find an active catalyst providing organic acids in a high selectivity in a green and natural solvent. Screening of the catalysts were carried out at 70 °C with H_2O_2 under atmospheric conditions in ethanol. The most active catalyst was tested in water (more environmentally friendly solvent) at 70–90 °C.

Experimental section

Materials

Glucose, magnesium nitrate hexahydrate (≥99%), aluminum nitrate nanohydrate (≥99%), strontium nitrate (≥99%), copper(II) chloride dehydrate, zinc(II) chloride

dehydrate, sodium orthovanadate and sodium hydroxide (97%) were purchased from Merck KGaA (Darmstadt, Germany). Cerium(III) chloride heptahydrate (99.9%) was purchased from Sigma-Aldrich. Sodium carbonate anhydrous (99%) and hydrogen peroxide (35%) were supplied by Isolab Chemicals (Wertheim, Germany).

Catalyst preparation

Metal(I)–metal(II) hydrotalcites were prepared by a co-precipitation method. Briefly, solution A was prepared by dissolving the two different metal salts in water. Solution B was 1 M NaOH aqueous solution. These two solutions were simultaneously added into aqueous sodium carbonate (Na_2CO_3) solution by dropwise at 58 °C and pH 11–12. After consumption of the metal solutions, the mixture was stirred for 1 h and left to be matured for 18 h. The resulting precipitates were filtered, washed with diluted water and dried at 80 °C for 18 h under vacuum. Obtained powder was then kept at 200 °C for 12 h. Some bimetallic oxides were calcined at 450 °C for 5 h with a heating rate of 3 °C/min. Prepared bimetallic oxides were labeled as: A–B; A refers to + 2 oxidation stage metals where B refers to + 3 oxidation stage metals. The calcined ones were labeled as A–B–cal.

Copper impregnation (5%) onto Mg–Al–cal catalyst were also performed with wet impregnation. Briefly, Mg–Al–cal was dispersed in water for 30 min under ultrasonication. The determined amount of $CuCl_2.2H_2O$ was dissolved in water. The resulting solution was added to the previous Mg–Al–cal suspension by dropwise at room temperature. The mixture was stirred for 1 h. This Cu loaded material were reduced by the addition of $NaBH_4$ in an iced bath. This mixture was then stirred for 1 h and left for aging. Obtained precipitate was filtered and dried at 150 °C for 10 h. The obtained catalyst was labeled as Cu/Mg–Al–cal–R.

Vanadium loading (5 wt%) to Mg–Al–cal was achieved by incipient wetness impregnation. The powder was directly calcined at 450 °C for 5 h. It was labeled as V/Mg–Al–cal.

Characterization of catalysts

The crystal phases and X-ray diffraction (XRD) patterns of the catalysts were analyzed with the Rigaku Smartlab instrument. The patterns were scanned between $2\theta = 5$–90° angles where the scanning speed was 3°/s. A wavelength of $\lambda = 0.15418$ nm and a power of 45 kV/40 mA of Cu K_α beam source was used. FT-IR measurements of the catalysts were performed with Perkin-Elmer Paragon 1000 model Fourier Transform Infrared Spectroscopy (FT-IR/ATR). Measurements were taken with a powder sample between 400 and 4000 cm^{-1}. Nitrogen physisorption analyzes were performed with the Quantachrome Autosorb IQ2 model instrument. All samples were degassed at 120 °C for 8 h prior to adsorption. The multipoint adsorption data were obtained at 77 K and relative pressure of 760 mmHg. The surface area, pore structures, and pore volumes of the catalysts were determined by the BET method.

Catalyst screening tests

Glucose oxidation tests were performed in glass reactor equipped with condenser at 70 °C for 6 h in ethanol and water. Hydrogen peroxide solution (35%) was used as an oxidant in the catalyst system. Briefly, 1.6 wt % of glucose was loaded into the reactor where catalyst/glucose ratio was 1/2. The mixture was stirred at 750 rpm in an oil bath with a magnetic stirrer. Excess O_2 gas was allowed to be left from the reactor during the reaction. Following the completion of reaction, reactor was cooled immediately in an ice bath and each sample was filtered with a 0.45 μm PVDF syringe filter and diluted for HPLC analysis.

Parametric studies

The effects of calcination (450 °C) were investigated with the most active catalysts. The reaction temperature (60, 70, 80 and 90 °C) was also studied with the most efficient catalyst in water medium.

Product analysis

The diluted samples were analyzed by Thermo Ultimate 3000 model high pressure liquid chromatography (HPLC) equipped with ICSep Coregel 87H3 (300×7.8 mm) organic acid column, UV–Visible (UV–Vis) and refractive index (RI) detectors. The injection volume was 20 μl. Dilute sulfuric acid (8 mM) was used as the mobile phase. The flow rate was 0.6 ml/min, where the column temperature was 60 °C and the RID temperature was 45 °C. Organic acids (gluconic acid, oxalic acid and levulinic acid etc.), aldehydes and furans were determined by UV–Vis detector while sugar (glucose and fructose) concentrations by RID detector.

Glucose conversion (X), product carbon-yield (Y) and carbon-selectivity (S) were calculated using the following equations.

$$X(\%) = \frac{\text{Moles of Glucose}_{in} - \text{Moles of Glucose}_{out}}{\text{Moles of Glucose}_{in}} \times 100$$

$$Y(\%) = \frac{\text{Moles of the Product} \times \text{Number of Carbon in the Product}}{\text{Moles of Glucose}_{in} \times 6} \times 100$$

$$S(\%) = \frac{\text{Moles of the Product} \times \text{Number of Carbon in the Product}}{\text{Moles of Glucose Reacted} \times 6} \times 100$$

Results and discussion

Characterization of the synthesized catalysts

XRD patterns of the synthesized and dried metal oxides are given in Fig. 1. Sr–Fe exhibited almost pure $SrCO_3$ crystals without trivalent metals [39, 40]. This may be attributed to well dispersion of Fe ions in the structure or presence of very small Fe_3O_4 crystals (< 5 nm) which XRD could not detected. Mg–Al pattern indicated magnesium–aluminum layered double hydroxide (LDH) structure with just little $MgAl_2O_4$ crystals (spinel form). Higher extent of ZnO and lower extent of CeO_2 crystals were observed in Zn–Ce. Probably, larger ionic radius of Ce atom prevented the formation of bimetallic crystals. XRD patterns of the synthesized and calcined bimetallic oxides are given in Fig. 2. Calcination of Mg–Al converted its crystal structure from LDH to spinel form. Less amount of MgO crystals were observed in this catalyst. Crystallinity of Zn–Ce was improved by calcination and new CeO crystals were formed. The calcined Sr–Fe preserved its structure, at the meantime the crystallinity was increased significantly.

FT-IR spectrums of dried Mg–Al, calcined Mg–Al, calcined and reacted Mg–Al catalysts are given in Fig. 3. Absorption bands at 3400–3500 cm^{-1} was due to the physisorption between located interphase and metal–O–H. The sharp absorption bands at 2980 cm^{-1} were attributed to the CO_3^{-2}–H_2O stretching vibrations [41] by the hydrogen bonding of carbonate ions in Mg–Al structure [42]. The band between 1350 and 1380 cm^{-1} was also attributed to the CO_3^{-2}
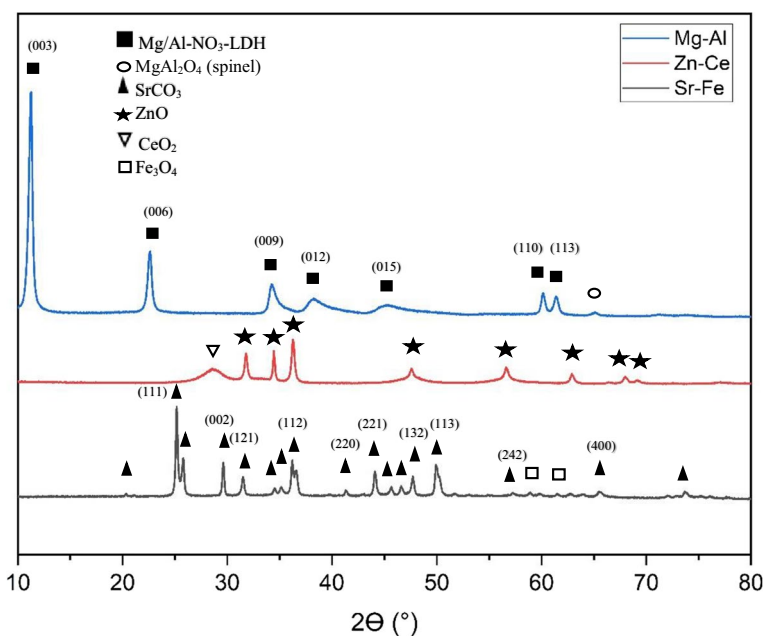

Fig. 1 XRD patterns of synthesized dried bimetallic oxides
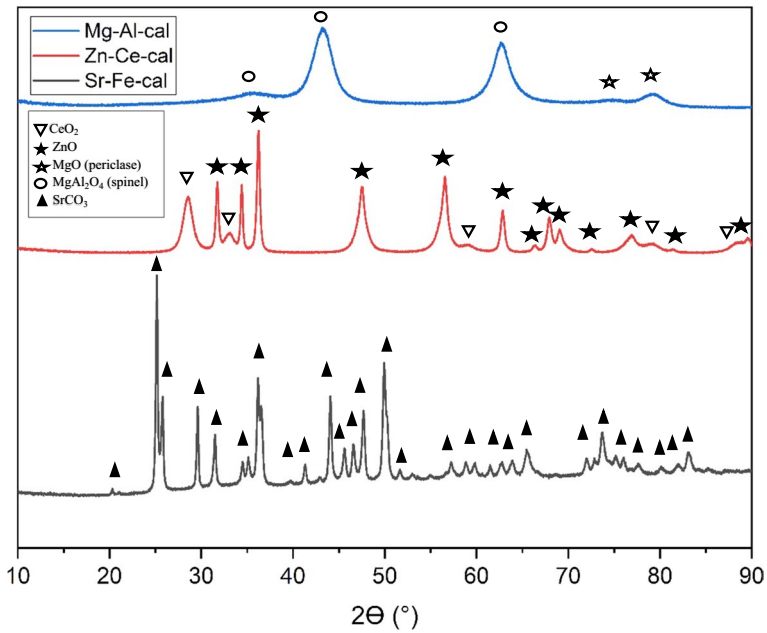
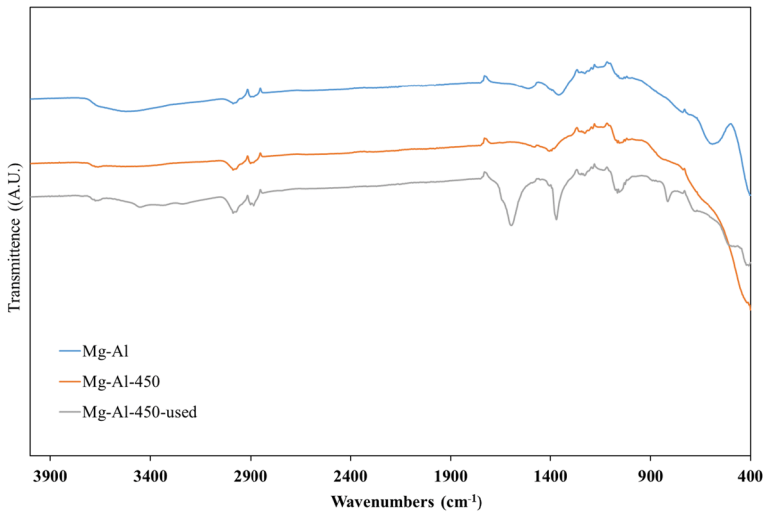**Fig. 2** XRD patterns of synthesized calcined bimetallic oxides

Fig. 3 FT-IR spectrums of synthesized bimetallic oxides

ions which was reduced slightly after calcination. However, there were still effective CO_3^{-2} groups in the structure even calcination process. Spinel structure prevented the leaving of CO_3^{-2} groups at high temperatures up to 500 °C. The used Mg–Al–450 catalyst indicated extra bands at 1621 and 1317 cm^{-1} which referred

to as carbonyl groups, emerged via the adsorption of products during reaction [43].

Textural properties of the synthesized catalysts are given in Table 1. The highest surface area was obtained with Mg-Ce, which was followed, by Mg–Al and Sr–Fe. Zn–Ce having very low surface area exhibited macroporous structure. None of the catalysts showed micropore area. The highest pore volume and large mesopores were obtained over Mg–Al catalyst that could provide the molecules to be easily adsorbed to the active centers.

Catalyst testing

The time dependent glucose conversions of the synthesized dried metal oxides are given in Fig. 4. Glucose conversion increased with the reaction time over all of the catalysts up to 4 h. Among the bimetallic oxides, the highest glucose conversion was achieved with Sr–Fe catalyst (approx. 30%). Sr–Fe provided high activity possibly depending on the presence of $SrCO_3$ crystals and its mesoporous structure. The alkali $SrCO_3$ crystal may have promoted the oxidation of glucose with Fe atoms; since the monometallic SrO without Fe, (prepared and tested in glucose oxidation -not given-) did not provide remarkable activity. The second highest conversion value was obtained with Zn–Ce. However, the conversion on this catalyst indicated a logarithmic trend up to 4 h then approached almost a constant value. The same trend was obtained over Mg–Al. At the end of the fourth hour, glucose conversion was obtained as 22.6% (approximately) and slightly dropped up to 6 h. This was due to the completion of H_2O_2 in 4–5 h over these catalysts. Afterwards, the catalyst took an action in reversible isomerization between glucose and fructose, fructose converted back to glucose. Some catalytic sites also may have been passivated by product adsorption in ethanol medium. IR results (Fig. 3) proved this product adsorption on to the catalyst surface. An increase in the conversion was observed very slow over Mg–Ce. Presumably, the peroxide decomposed as O_2, oxidizing the catalyst before it could oxidize the reactant, or quickly left without being able to oxidize it. CaO as a base catalyst was reported many times in literature promoting carbohydrate oxidation [26, 44, 45]. Accordingly, to examine the effect of base sites on glucose conversion, glucose oxidation reaction was also performed with CaO as comparison and 38% glucose conversion was provided.

Formic acid yields of the synthesized metal oxides are given in Fig. 5. The highest formic acid yield was obtained with Sr–Fe as ~5%. The yield of formic acid over

Catalysts	BET surface area (m²/g)	B.J.H. pore diameter (nm)	Pore volume (cm³/g)	External surface area (m²/g)
Sr–Fe	44.6	10.9	0.12	44.6
Mg–Al	56.9	45.1	0.64	56.9
Mg–Ce	78.1	20.6	0.41	78.1
Zn–Ce	12.0	59.2	0.18	12.0

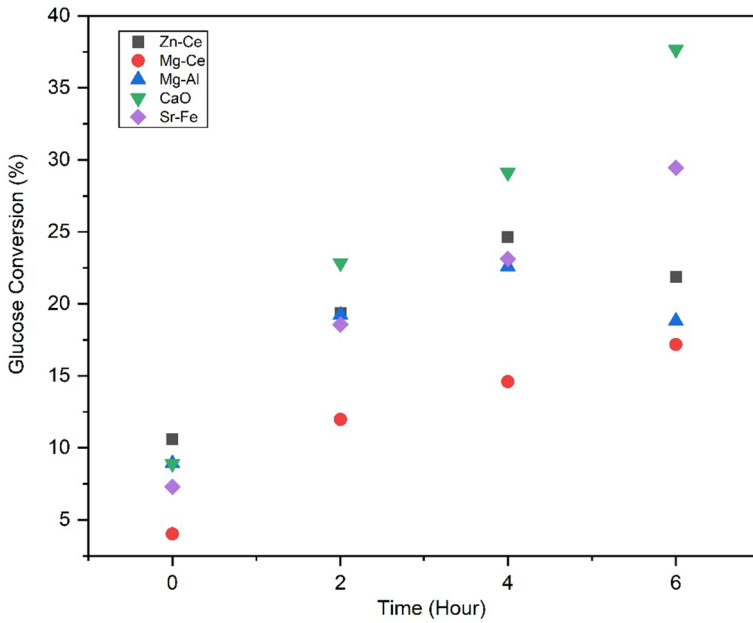Table 1 Textural properties of the synthesized bimetallic oxides

Fig. 4 Time dependent glucose conversions over metal oxides (Solvent: ethanol, Temperature: 70 °C, Time: 6 h, Catalyst/Glucose: 1/2, 1.6% Glucose, 250% H_2O_2 Solution)
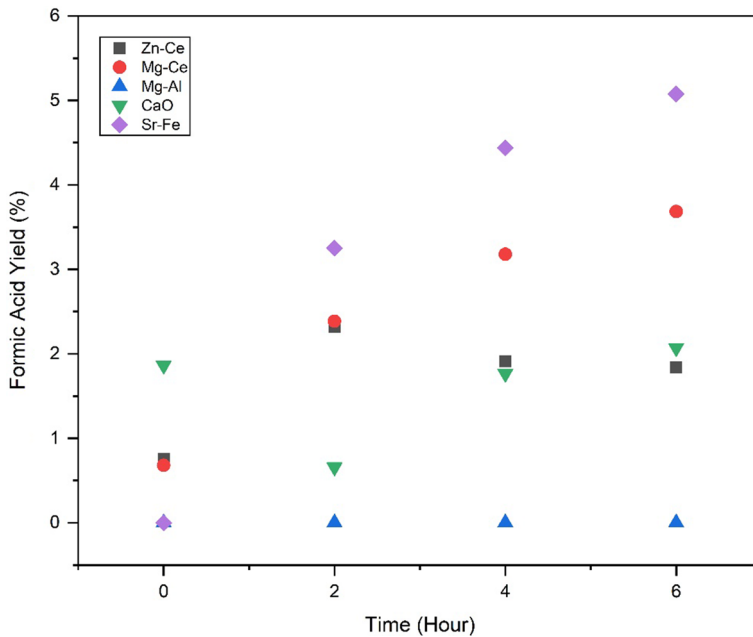

Fig. 5 Time dependent formic acid yield over metal oxides (Solvent: ethanol, Temperature: 70 °C, Time: 6 h, Catalyst/Glucose: 1/2, 1.6% Glucose, 250% H_2O_2 Solution)

CaO, which provided the highest activity, remained just around 2%. Mg–Al also did not form formic acid in the current form.

The detailed product distributions over all of the catalysts are given in Table 2. CaO was very active for the glucose conversion (38%) but it provided the only 3.7% lactic acid and 2.1% formic acid yields. Mg–Al was not effective for the production of formic acid; also, lactic acid yield was only around 2.7%. Considering the product distributions and low product yields of catalysts, it is revealed that neither catalyst exhibited high selectivity to any product. Probably, most of the glucose converted to CO_2 [46]. Therefore, some selected catalysts Mg–Al, Sr–Fe and Zn–Ce were calcined in order to improve their catalytic activities and product selectivities.

Glucose conversions of the calcined catalysts are given in Fig. 6. The results suggest that calcination significantly improved the catalytic activity of Mg–Al catalyst from 18.8 to 62.0%. Sr–Fe and Zn–Ce catalyst showed similar activities and tended to remain stable at around 20% levels. Probably, CO_3 groups in the structure of these catalysts were removed during calcination and activity dropped. However, CO_3 groups in Mg–Al were protected by the spinel structure, which was mentioned in characterization (FT-IR) part. Although the calcination recreates new reactive centers and enables them to show higher activity, in some conditions, it causes the active centers to be trapped inside the pores. This obstructs the accessibility of these centers for reactants. Also, the crystal size of the calcined catalysts may increase due to sintering, which eliminates the possibility of good contact between the reactant and the active surfaces [47].

The formic acid yields over the calcined catalysts are given in Fig. S1. The highest formic acid yield was obtained with Mg–Al–cal as 10.2%. Formic acid yield obtained with Sr–Fe–cal, and Zn–Ce–cal catalysts remained below 5%. According to the results, the most effective catalyst, in terms of the formic acid yields, was determined as calcined Mg–Al. Mg and Al, among synthesized 10 different bimetallic oxides, formed a synergistic combination in the spinel structure and became effective after calcination for the production of formic acid. In order to check the oxidation possibility of ethanol during reaction, an ethanol oxidation test was carried out with Mg–Al–cal at the same conditions in the absence of the glucose. Formation of any aldehydes or oxidation products were not detected in HPLC–UV analysis. This check was proved that Mg–Al–cal catalyzes the glucose only.

The product distributions of the calcined catalysts are given in Table 3. Mg–Al–cal also favored the retro–aldol condensation pathway as well as formic acid formation in alcohol medium and 6.8% of lactic acid was formed as a by-product [48]. Zn–Ce–cal and Sr–Fe–cal catalysts showed similar activities. On these catalysts, the glucose was converted to formic (3%) and acetic acids (2.8%).

Effects of Cu and V loading to Mg–Al–cal on glucose conversion and product selectivities were also investigated. The time dependent glucose conversions are given in Fig. 7. Metal loadings reduced the catalytic activity significantly. Interestingly, the Cu loaded-reduced catalyst did not provide remarkable activity up to 4 h, then increased rapidly to 45% in 2 h. CuO, having effective oxidative potential, was reported to have promoted the oxidation of carbohydrates previously [49–51].

Table 2 Product distributions over synthesized metal oxides

Catalyst	Conversion (%) Glucose	Yield (%) Fructose	Formic acid	Acetic acid	Gluconic acid	Glyceraldehyde	Glycolic acid	DHA	Lactic acid
Zn–Ce	21.9	0.3	1.8	0.5	0.3	0.5	0.7	–	1.1
Sr–Fe	29.4	–	5.1	1.5	0.0	0.8	–	–	2.6
Mg–Ce	17.2	–	3.7	–	–	0.5	0.7	–	1.0
Mg–Al	18.8	–	–	–	–	0.7	0.7	–	2.7
CaO	38.0	–	2.1	–	–	–	–	–	3.7

Solvent: ethanol, Temperature: 70 °C, Time: 6 h, Catalyst/Glucose:1/2, 1.6% Glucose, 250% H_2O_2 solution
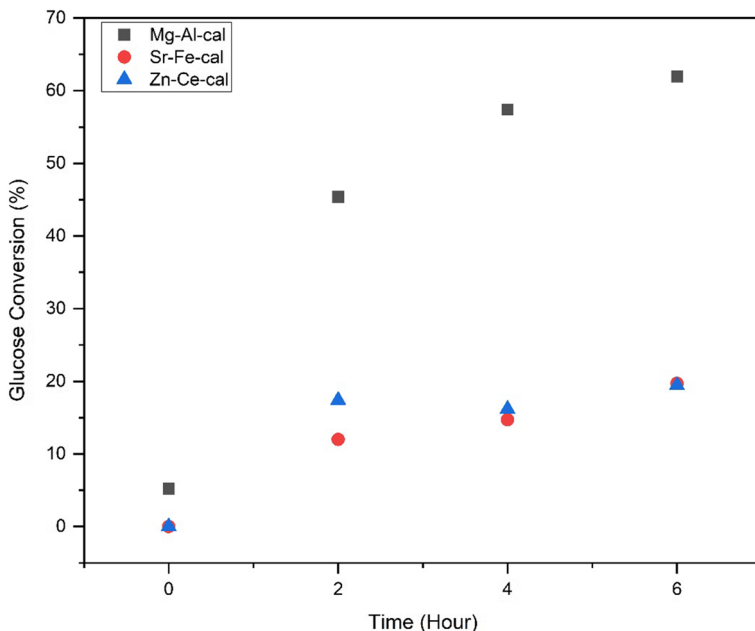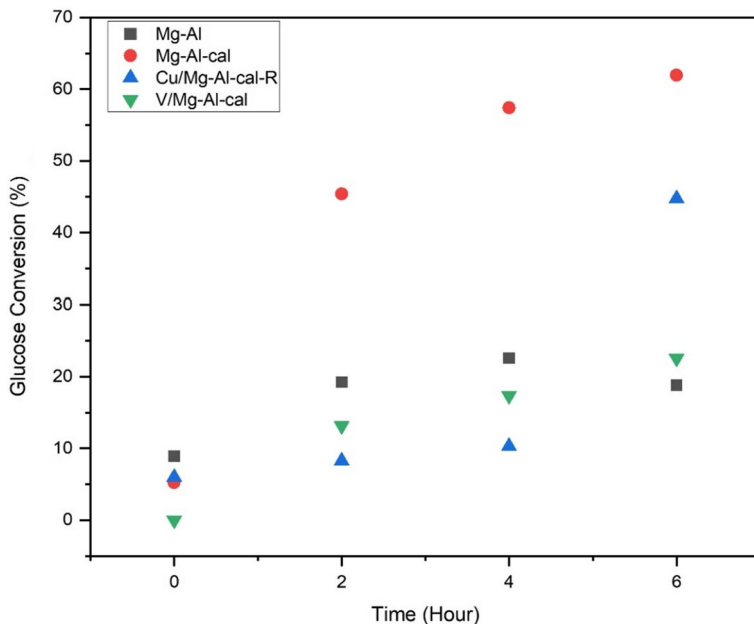
Fig. 6 Glucose conversions over calcined bimetallic oxides (Solvent: ethanol, Temperature: 70 °C, Time: 6 h, Catalyst/Glucose: 1/2, 1.6% Glucose, 250% H_2O_2 Solution)

Effects of metal loading on formic acid yields are given in Fig. S2. Mg–Al–cal and Cu/Mg–Al–cal–R exhibited similar formic acid yields at 6 h. The formic acid yield on Cu/Mg–Al–cal–R was very low at 4 h; however, it exhibited a significant jump at 6 h. Only 3.9% of formic acid could be obtained with V/Mg–Al–cal catalyst. Since Mg–Al–cal does not have a very high surface area, the loaded vanadium may have narrowed the active centers or may have not been distributed homogenously.

The product distributions of Cu and V loaded Mg–Al–cal catalysts are given in Table 4. When the glucose conversion on Cu/Mg–Al–cal–R was 45%, acetic and formic acid yields were 25.5% and 10.4%, respectively. This means that Cu/Mg–Al–cal–R catalyst provided a high selectivity (~57%) to acetic acid and also very high selectivity (~85%) to total organic acids. On the other hand, the formic and lactic acid yields over V/Mg–Al–cal were just obtained as 3.9 and 2.5%, respectively.

Through these results, the highest glucose conversion and formic acid selectivity were obtained with Mg–Al–cal. Therefore, Mg–Al–cal catalyst was tested in glucose oxidation in water environment at different temperatures (60, 70, 80 and 90 °C) for 6 h. Obtained results are given in Fig. 8. Glucose conversion increased with the increase in temperature and the highest glucose conversion was found as ~40% at 90 °C. The lowest glucose conversion at 6 h was obtained as 22.5% at 60 °C. At 90 °C, drop in conversion was observed after 4 h which was due to the reversible isomerization between glucose and fructose as mentioned before.

Table 3 Product distributions over calcined bimetallic oxides

Catalyst	Conversion (%) Glucose	Yield (%) Fructose	Formic acid	Acetic acid	Gluconic acid	Glyceraldehyde	Glycolic acid	DHA	Lactic acid
Zn–Ce–cal	19.5	0.3	3.0	2.8	–	0.5	0.6	0.4	1.3
Sr–Fe–cal	19.7	–	3.6	2.8	–	0.5	–	–	1.6
Mg–Al–cal	62.0	0.2	10.2	–	–	1.5	0.4	–	6.8

Solvent: ethanol, Temperature: 70 °C, Time: 6 h, Catalyst/Glucose:1/2, 1.6% Glucose Loading, 250% H_2O_2 solution

Fig. 7 Glucose conversions over functionalized Mg–Al–cal (Solvent: ethanol, Temperature: 70 °C, Time: 6 h, Catalyst/Glucose: 1/2, 1.6% glucose loading, 250% H_2O_2 solution)

The product selectivities of the Mg–Al–cal at different temperatures are also given in Fig. 8. As the temperature increased, the total organic acid selectivity increased. At 90 °C, about 98% organic acid selectivity was obtained in water. This proved that the catalyst also showed higher selectivities to organic acids in an aqueous environment. It is also revealed that acetic acid was formed at higher temperatures, but at low temperature (60 °C) lactic acid was formed via condensation route.

Mg–Al–cal catalyst was also tested in the presence of formic acid in ethanol medium to investigate catalyst deactivation by product adsorption. The time-dependent glucose conversions and product yields are given in Fig. 9. Without formic acid addition, glucose conversion was obtained as 62%, while in the presence of formic acid, it was reduced to 51%. This was due to the passivation of some active sites by product adsorption as previously indicated in Fig. 3. On the other hand, formic acid and ethanol medium caused a change in the reaction pathway. Interestingly, high amount of levulinic acid produced through glucose dehydration. In the literature, glucose is isomerized to fructose on the base centers, which is followed by the dehydration of fructose to levulinic acid over acid sites. Herein, formic acid acted as homogeneous acid catalyst and formed levulinic acid with Mg–Al–cal. This shows that Mg–Al-cal catalyst can be a good alternative for different reaction pathways in different mediums.

Table 4 Product distributions over functionalized Mg–Al–cals

| Catalyst | Conversion (%) | Yield (%) | | | | | | | |
	Glucose	Fructose	Formic acid	Acetic acid	Gluconic acid	Glyceraldehyde	Glycolic acid	Lactic acid
Mg–Al	18.8	–	–	–	–	0.7	0.7	2.7
Mg–Al–cal	62.0	0.2	10.2	–	–	1.5	0.4	6.8
Cu/Mg–Al–calR	45.0	–	10.4	25.5	0.3	0.3	0.4	1.5
V/Mg–Al–cal	23.0	–	3.9	–	–	–	1.3	2.5

Solvent: ethanol, Temperature: 70 °C, Time: 6 h, Catalyst/Glucose: 1/2, 1.6% Glucose, 250% H_2O_2 solution
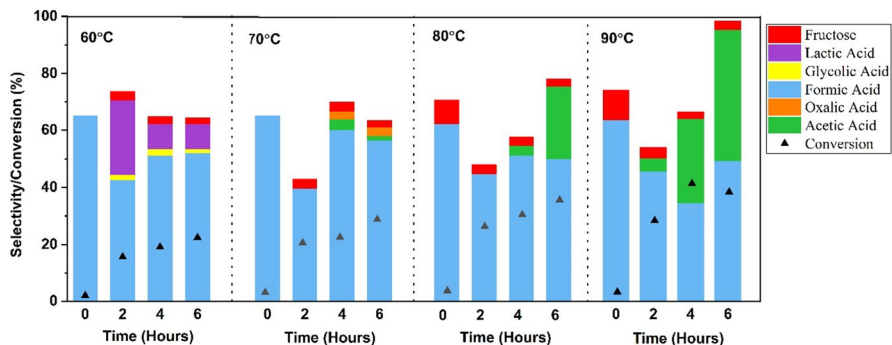
Fig. 8 Glucose conversion and product selectivities over Mg–Al–cal at different reaction temperatures in water (Solvent: water. Time: 6 h, Catalyst/Glucose: 1/2, 1.6% glucose, 250% H$_2$O$_2$ solution). (Color figure online)
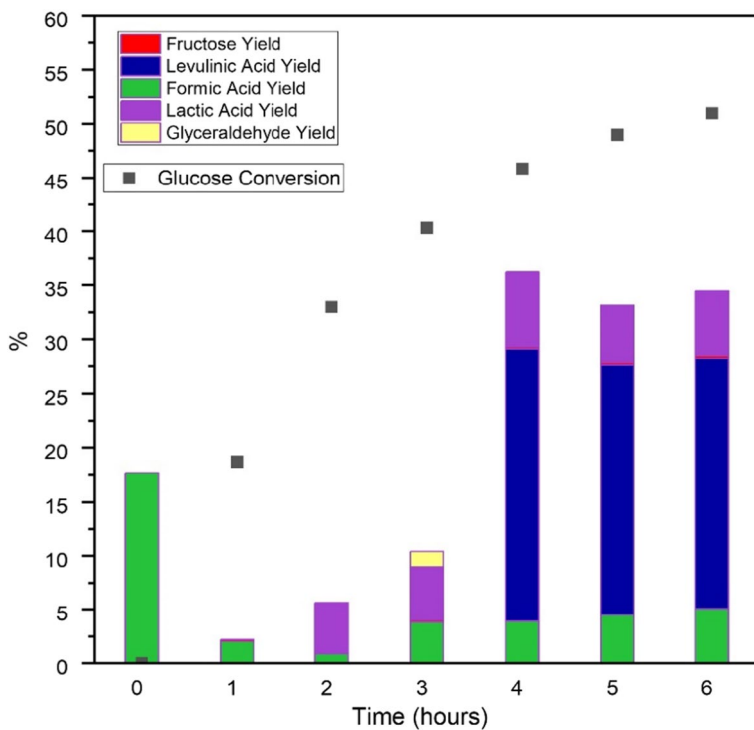

Fig. 9 Glucose conversion and product yields of the experiment performed by adding formic acid to Mg–Al–cal (Solvent: ethanol, Time: 6 h, Catalyst/Glucose: 1/2, 1.6% glucose). (Color figure online)

Conclusions

Glucose oxidation to formic and acetic acids was successfully achieved over spinel and LDH form bimetallic oxides. Mg–Al was found completely in LDH and spinel structure. The Mg–Al–cal, the most effective catalyst in EtOH, exhibited 60% of glucose conversion where the formic acid selectivity was 10.2%. Bi-functional properties (base sites and redox sites) of this catalyst facilitated the H_2O_2 decomposition and oxidation of glucose. Promising performances as well as high formic and acetic acid selectivities via oxidation (95% total organic acid selectivity at 38% glucose conversion) were obtained with Mg–Al–cal in water at 90 °C. This catalyst also exhibited impressive total organic acid (TOA) selectivity in dehydration route at 4 h. Deactivation studies (by product adsorption) were investigated with the addition of formic acid to the reaction medium in ethanol and deactivation was not observed in 6 h. In this medium, Mg–Al–cal provided 78% total TOA selectivity (levulinic acid + lactic acid + formic acid) in ethanol at very low temperature (70 °C) under atmospheric pressure.

Author contributions The manuscript was written through contributions of all authors. All authors have given approval to the final version of the manuscript. All of the authors contributed equally.

Data availability we confirm that the data supporting the findings of this study are available within the article and its supplementary materials.

References

1. Shi S, Yin J (2021) Global research on carbon footprint: a scientometric review. Environ Impact Assess Rev 89:106571. https://doi.org/10.1016/j.eiar.2021.106571
2. Kim Y, Mittal A, Robichaud DJ et al (2020) Prediction of hydroxymethylfurfural yield in glucose conversion through investigation of lewis acid and organic solvent effects. ACS Catal 10:14707–14721. https://doi.org/10.1021/acscatal.0c04245
3. Xu J, Zhao Y, Xu H et al (2014) Selective oxidation of glycerol to formic acid catalyzed by Ru(OH)$_4$/r-GO in the presence of FeCl$_3$. Appl Catal B 154–155:267–273. https://doi.org/10.1016/j.apcatb.2014.02.034
4. Sanpitakseree C, Motagamwala AH, Dumesic JA, Neurock M (2022) Solvent and chloride ion effects on the acid-catalyzed conversion of glucose to 5-hydroxymethylfurfural. ACS Sustain Chem Eng. https://doi.org/10.1021/acssuschemeng.2c00651
5. Lu T, Hou Y, Wu W et al (2018) Formic acid and acetic acid production from corn cob by catalytic oxidation using O$_2$. Fuel Process Technol 171:133–139. https://doi.org/10.1016/j.fuproc.2017.11.010

6. Gromov NV, Taran OP, Delidovich IV et al (2016) Hydrolytic oxidation of cellulose to formic acid in the presence of Mo–V–P heteropoly acid catalysts. Catal Today 278:74–81. https://doi.org/10.1016/j.cattod.2016.03.030

7. Franz S, Shcherban ND, Simakova IL et al (2021) Oxidation of glucose and arabinose mixtures over Au/Al$_2$O$_3$. Reac Kinet Mech Cat 132:59–72. https://doi.org/10.1007/s11144-020-01901-w

8. Melero JA, Moreno J, Iglesias J et al (2020) Ru-ZrO2-SBA-15 as efficient and robust catalyst for the aqueous phase hydrogenation of glucose to sorbitol. Mol Catal 484:110802. https://doi.org/10.1016/J.MCAT.2020.110802

9. Murzin DY, Murzina EV, Tokarev A et al (2015) Arabinogalactan hydrolysis and hydrolytic hydrogenation using functionalized carbon materials. Catal Today 257:169–176. https://doi.org/10.1016/j.cattod.2014.07.019

10. Pan J, Li J, Wang C, Yang Z (2007) Multi-wall carbon nanotubes supported ruthenium for glucose hydrogenation to sorbitol. React Kinet Catal Lett 90:233–242. https://doi.org/10.1007/s11144-007-4989-4

11. Candu N, El Fergani M, Verziu M et al (2019) Efficient glucose dehydration to HMF onto Nb-BEA catalysts. Catal Today 325:109–116. https://doi.org/10.1016/j.cattod.2018.08.004

12. Zhang Y, Li B, Wei Y et al (2019) Direct synthesis of metal-organic frameworks catalysts with tunable acid–base strength for glucose dehydration to 5-hydroxymethylfurfural. J Taiwan Inst Chem Eng 96:93–103. https://doi.org/10.1016/j.jtice.2018.12.020

13. Shen Z, Chen W, Zhang W et al (2022) Efficient catalytic conversion of glucose into lactic acid over Y-β and Yb-β zeolites. ACS Omega 7:25200–25209. https://doi.org/10.1021/acsomega.2c02051

14. Ponce S, Wesinger S, Ona D et al (2021) Valorization of secondary feedstocks from the agroindustry by selective catalytic oxidation to formic and acetic acid using the OxFA process. Biomass Convers Biorefinery. https://doi.org/10.1007/s13399-021-01854-7

15. Lu T, Hou Y, Wu W et al (2018) Catalytic oxidation of cellulose to formic acid in V(V)-Fe(III)-H$_2$SO$_4$ aqueous solution with O$_2$. Fuel Process Technol 173:197–204. https://doi.org/10.1016/j.fuproc.2018.02.001

16. Sato R, Choudhary H, Nishimura S, Ebitani K (2015) Synthesis of formic acid from monosaccharides using calcined Mg–Al hydrotalcite as reusable catalyst in the presence of aqueous hydrogen peroxide. Org Process Res Dev 19:449–453. https://doi.org/10.1021/op5004083

17. Lee J, Saha B, Vlachos DG (2016) Pt catalysts for efficient aerobic oxidation of glucose to glucaric acid in water. Green Chem 18:3815–3822. https://doi.org/10.1039/c6gc00460a

18. Zhang Z, Huber GW (2018) Catalytic oxidation of carbohydrates into organic acids and furan chemicals. Chem Soc Rev 47:1351–1390. https://doi.org/10.1039/c7cs00213k

19. Önal Y, Schimpf S, Claus P (2004) Structure sensitivity and kinetics of ᴅ-glucose oxidation to ᴅ-gluconic acid over carbon-supported gold catalysts. J Catal 223:122–133. https://doi.org/10.1016/j.jcat.2004.01.010

20. Sheet SD (2017) Formic acid formic acid. ICIS Chem Bus 1:1–12. https://doi.org/10.1002/14356007.a12

21. Boddien A, Mellmann D, Gärtner F et al (2011) Efficient dehydrogenation of formic acid using an iron catalyst. Science 333:1733–1736. https://doi.org/10.1126/science.1206613

22. Pérez-Fortes M, Schöneberger JC, Boulamanti A et al (2016) Formic acid synthesis using CO2 as raw material: techno-economic and environmental evaluation and market potential. Int J Hydrog Energy 41:16444–16462. https://doi.org/10.1016/j.ijhydene.2016.05.199

23. Medrano-García JD, Ruiz-Femenia R, Caballero JA (2019) Revisiting classic acetic acid synthesis: optimal hydrogen consumption and carbon dioxide utilization, vol 46. Elsevier, Masson SAS, pp 145–150

24. Hitt F (2003) Le caractère fonctionnel des représentations. Ann didacqique Sci Cogn 8:255–271. https://doi.org/10.1002/14356007.a01

25. Wölfel R, Taccardi N, Bösmann A, Wasserscheid P (2011) Selective catalytic conversion of biobased carbohydrates to formic acid using molecular oxygen. Green Chem 13:2759–2763. https://doi.org/10.1039/c1gc15434f

26. Tang Z, Deng W, Wang Y et al (2014) Transformation of cellulose and its derived carbohydrates into formic and lactic acids catalyzed by vanadyl cations. Chemsuschem 7:1557–1567

27. Wang W, Niu M, Hou Y et al (2014) Catalytic conversion of biomass-derived carbohydrates to formic acid using molecular oxygen. Green Chem 16:2614. https://doi.org/10.1039/c4gc00145a

28. He R, Ma T, Cheng J et al (2021) Formation of formic acid from glucose with simultaneous conversion of Ag_2O to Ag under mild hydrothermal conditions. ACS Omega 6:11260–11265. https://doi.org/10.1021/acsomega.1c00106

29. Wang C, Chen X, Qi M et al (2019) Room temperature, near-quantitative conversion of glucose into formic acid. Green Chem 21:6089–6096. https://doi.org/10.1039/c9gc02201e

30. Niu M, Hou Y, Wu W et al (2018) Successive C1–C2 bond cleavage: the mechanism of vanadium(v)-catalyzed aerobic oxidation of d-glucose to formic acid in aqueous solution. Phys Chem Chem Phys 20:17942–17951. https://doi.org/10.1039/c8cp02352b

31. Tathod A, Kane T, Sanil ES, Dhepe PL (2014) Solid base supported metal catalysts for the oxidation and hydrogenation of sugars. J Mol Catal A 388–389:90–99. https://doi.org/10.1016/j.molcata.2013.09.014

32. Megías-Sayago C, Bobadilla LF, Ivanova S et al (2018) Gold catalyst recycling study in base-free glucose oxidation reaction. Catal Today 301:72–77. https://doi.org/10.1016/j.cattod.2017.03.022

33. Miedziak PJ, Alshammari H, Kondrat SA et al (2014) Base-free glucose oxidation using air with supported gold catalysts. Green Chem 16:3132–3141. https://doi.org/10.1039/c4gc00087k

34. Kwon D, Kang JY, An S et al (2020) Tuning the base properties of Mg–Al hydrotalcite catalysts using their memory effect. J Energy Chem 46:229–236. https://doi.org/10.1016/j.jechem.2019.11.013

35. Mobley JK, Crocker M (2015) Catalytic oxidation of alcohols to carbonyl compounds over hydrotalcite and hydrotalcite-supported catalysts. RSC Adv 5:65780–65797. https://doi.org/10.1039/c5ra11254k

36. Kılıç HA, Kılıç E, Erden L, Gök Y (2022) Highly selective oxidation of glucose to formic acid over synthesized hydrotalcite—like catalysts under base free mild conditions. Res Chem Intermed. https://doi.org/10.1007/s11164-022-04811-9

37. Choudhary VR, Dumbre DK, Uphade BS, Narkhede VS (2004) Solvent-free oxidation of benzyl alcohol to benzaldehyde by tert-butyl hydroperoxide using transition metal containing layered double hydroxides and/or mixed hydroxides. J Mol Catal A 215:129–135. https://doi.org/10.1016/j.molcata.2004.01.009

38. Zou X, Goswami A, Asefa T (2013) Efficient noble metal-free (electro)catalysis of water and alcohol oxidations by zinc-cobalt layered double hydroxide. J Am Chem Soc 135:17242–17245. https://doi.org/10.1021/ja407174u

39. Qian WY, Sun DM, Zhu RR et al (2012) pH-sensitive strontium carbonate nanoparticles as new anticancer vehicles for controlled etoposide release. Int J Nanomed 7:5781–5792. https://doi.org/10.2147/IJN.S34773

40. Efthimiopoulos I, Müller J, Winkler B et al (2019) Vibrational response of strontianite at high pressures and high temperatures and construction of P-T phase diagram. Phys Chem Miner 46:27–35. https://doi.org/10.1007/s00269-018-0984-8

41. Zeng RC, Li XT, Liu ZG et al (2015) Corrosion resistance of Zn–Al layered double hydroxide/poly(lactic acid) composite coating on magnesium alloy AZ31. Front Mater Sci 9:355–365. https://doi.org/10.1007/s11706-015-0307-7

42. Kostura B, Matýsek D, Kukutschová J, Leško J (2012) Phosphate interaction with calcined form of Mg–Al–CO_3 hydrotalcite in aqueous solutions. Ann Chim Sci des Mater 37:11–20. https://doi.org/10.3166/acsm.37.11-20

43. Prananto YP, Khunur MM, Wahyuni DT et al (2013) Study of gel growth cobalt (ii) oxalate crystals as precursor of CO $3O_4$ nano particles. Bull Chem React Eng Catal 7:198–204. https://doi.org/10.9767/bcrec.7.3.4066.198-204

44. Taufiq-Yap YH, Lee HV, Hussein MZ, Yunus R (2011) Calcium-based mixed oxide catalysts for methanolysis of *Jatropha curcas* oil to biodiesel. Biomass Bioenerg 35:827–834. https://doi.org/10.1016/j.biombioe.2010.11.011

45. Steinbach D, Klier A, Kruse A et al (2020) Isomerization of glucose to fructose in hydrolysates from lignocellulosic biomass using hydrotalcite. Processes 8:1–15. https://doi.org/10.3390/PR8060644

46. Lu T, Hou Y, Wu W et al (2018) Catalytic oxidation of biomass to oxygenated chemicals with exceptionally high yields using H5PV2Mo10O40. Fuel 216:572–578. https://doi.org/10.1016/j.fuel.2017.12.044

47. Zhang J, Wu S, Liu Y, Li B (2013) Hydrogenation of glucose over reduced Ni/Cu/Al hydrotalcite precursors. Catal Commun 35:23–26. https://doi.org/10.1016/j.catcom.2013.01.017

48. Doungsri S, Rattanaphanee P, Wongkoblap A (2019) Production of lactic acid from cellulose using solid catalyst. MATEC Web Conf 268:07006. https://doi.org/10.1051/matecconf/201926807006
49. Wang F, Wang Y, Jin F et al (2014) One-pot hydrothermal conversion of cellulose into organic acids with cuo as an oxidant. Ind Eng Chem Res 53:7939–7946. https://doi.org/10.1021/ie404311d
50. Yao GD, Huo ZB, Jin FM (2011) Direct reduction of copper oxide into copper under hydrothermal conditions. Res Chem Intermed 37:351–358. https://doi.org/10.1007/s11164-011-0258-2
51. Li Q, Yao G, Zeng X et al (2012) Facile and green production of Cu from CuO using cellulose under hydrothermal conditions. Ind Eng Chem Res 51:3129–3136. https://doi.org/10.1021/ie202151s